J Neurophysiol 113: 3943–3953, 2015.
First published April 8, 2015; doi:10.1152/jn.01055.2014.

Closed-loop, ultraprecise, automated craniotomies

Nikita Pak,[1,2] Joshua H. Siegle,[3]* Justin P. Kinney,[1]* Daniel J. Denman,[3] Timothy J. Blanche,[3] and Edward S. Boyden[1]

[1]*Media Lab and McGovern Institute, Departments of Biological Engineering and Brain and Cognitive Sciences, Massachusetts Institute of Technology, Cambridge, Massachusetts;* [2]*Department of Mechanical Engineering, Massachusetts Institute of Technology, Cambridge, Massachusetts; and* [3]*Allen Institute for Brain Science, Seattle, Washington*

Submitted 26 December 2014; accepted in final form 7 April 2015

Pak N, Siegle JH, Kinney JP, Denman DJ, Blanche TJ, Boyden ES. Closed-loop, ultraprecise, automated craniotomies. *J Neurophysiol* 113: 3943–3953, 2015. First published April 8, 2015; doi:10.1152/jn.01055.2014.—A large array of neuroscientific techniques, including in vivo electrophysiology, two-photon imaging, optogenetics, lesions, and microdialysis, require access to the brain through the skull. Ideally, the necessary craniotomies could be performed in a repeatable and automated fashion, without damaging the underlying brain tissue. Here we report that when drilling through the skull a stereotypical increase in conductance can be observed when the drill bit passes through the skull base. We present an architecture for a robotic device that can perform this algorithm, along with two implementations—one based on homebuilt hardware and one based on commercially available hardware—that can automatically detect such changes and create large numbers of precise craniotomies, even in a single skull. We also show that this technique can be adapted to automatically drill cranial windows several millimeters in diameter. Such robots will not only be useful for helping neuroscientists perform both small and large craniotomies more reliably but can also be used to create precisely aligned arrays of craniotomies with stereotaxic registration to standard brain atlases that would be difficult to drill by hand.

automation; cranial windows; craniotomy; robotics

AUTOMATION OF CRANIOTOMIES could in principle enable in vivo neuroscience experiments to be performed with greater ease, reproducibility, and throughput than is possible by human surgical operators. These benefits could in turn result in better repeatability of experiments and higher-quality neural data, as well as the ability to deploy neural recording or stimulation probes in complex three-dimensional (3D) geometries that target multiple brain regions (Zorzos et al. 2012). We earlier automated in vivo whole cell patch-clamp neural recording (Kodandaramaiah et al. 2012), discovering that a glass micropipette being lowered into the living mouse brain underwent a stereotyped increase in pipette resistance upon encountering a cell, which enabled us to build a robot that could automatically patch clamp neurons in the living mammalian brain. We hypothesized that an analogous approach, lowering a drill through the skull until an increase in the conductance between the drill and the body indicated that the drill was through the skull, may be of use in automating craniotomy surgeries. We found that this was the case: a sudden increase in the electrical conductance between the drill and the body indicated when the drill was through the skull but not touching the brain.

We developed an algorithm based on this discovery, implemented a robot to perform automated craniotomies using conductance measurements, and implemented a nonpointed drill bit strategy (i.e., using a square end mill) to completely eliminate brain bleeding during surgery. Next, we outfitted a commercially available (see METHODS) motorized stereotaxic apparatus with a measurement circuit based on the same principle. Using the same detection algorithm, we were able to create larger windows in the skull by drilling multiple small craniotomies in a ring, interpolating between them, and removing the skull piece thus isolated. Robots utilizing this approach may find widespread use for in vivo neuroscience experiments that require large cranial windows or multisite injector, electrode, fiber, or other device insertion through arrays of craniotomies.

METHODS

Homebuilt system: overview. We developed a homebuilt system to evaluate the concept, so that we could rapidly customize it for evaluating various key parameters. This is the system that we used in Figs. 1–3. Later, we sought to see whether our algorithm, with some minor hardware modifications, could be adapted to run on a commercial motorized stereotax; that system is used in Figs. 4 and 5 (see below). The homebuilt system consisted of an air-powered dental drill (PR-304, NSK, Tokyo, Japan) mounted on a three-axis computer-controlled stage equipped with three motors (PT3/M-Z8 stage, TDC001 controllers, TCH002 power supply, Thorlabs, Newton, NJ), using a 3D-printed, electrically insulating mount made of acrylonitrile butadiene styrene (ABS), with an electric potential detection circuit running through the drill (Fig. 1, *A–C*). Parts lists, software, and photographs for the homebuilt device (and also for the modified commercial stereotax; see below) can be obtained from **http://autosurgery.org**.

Homebuilt system: electrical circuit. In the homebuilt system, the electric potential circuit worked by sending a sine wave through a sense resistor and the body of the animal and finally to a measurement device (Fig. 1*A*). Since the homebuilt robot was used for initial, exploratory experiments, different combinations of signal sources, sense resistances, means of creating electrical contact to the animal, cables, and measurement devices were used. This information has been summarized in Table 1 for reference (along with key parameters for the modified commercial stereotax; see below). When the coaxial and USB cables (see Table 1 to see which experiments used the coaxial vs. USB cables) were used, their wire mesh shields connected to earth ground to minimize the effects of environmental noise. In all cases, the rear paw of the mouse made electrical contact to the ground lead of the cable connected to the measurement device through a piece of metal (contact area of 5 mm^2) touching the skin of the paw and held stationary by a test clip whose spring had been stretched to make it weaker, so as not to injure the animal. (Conductive gels may in principle facilitate this safe connectivity, but we did not find it necessary here.) The recommended configuration for end-user automated craniotomies is as used to generate the data for Fig. 3, *F* and *G*.

* J. H. Siegle and J. P. Kinney contributed equally to this work.
Address for reprint requests and other correspondence: Edward S. Boyden, E15-421, 20 Ames St., Cambridge, MA 02139 (e-mail: esb@media.mit.edu).

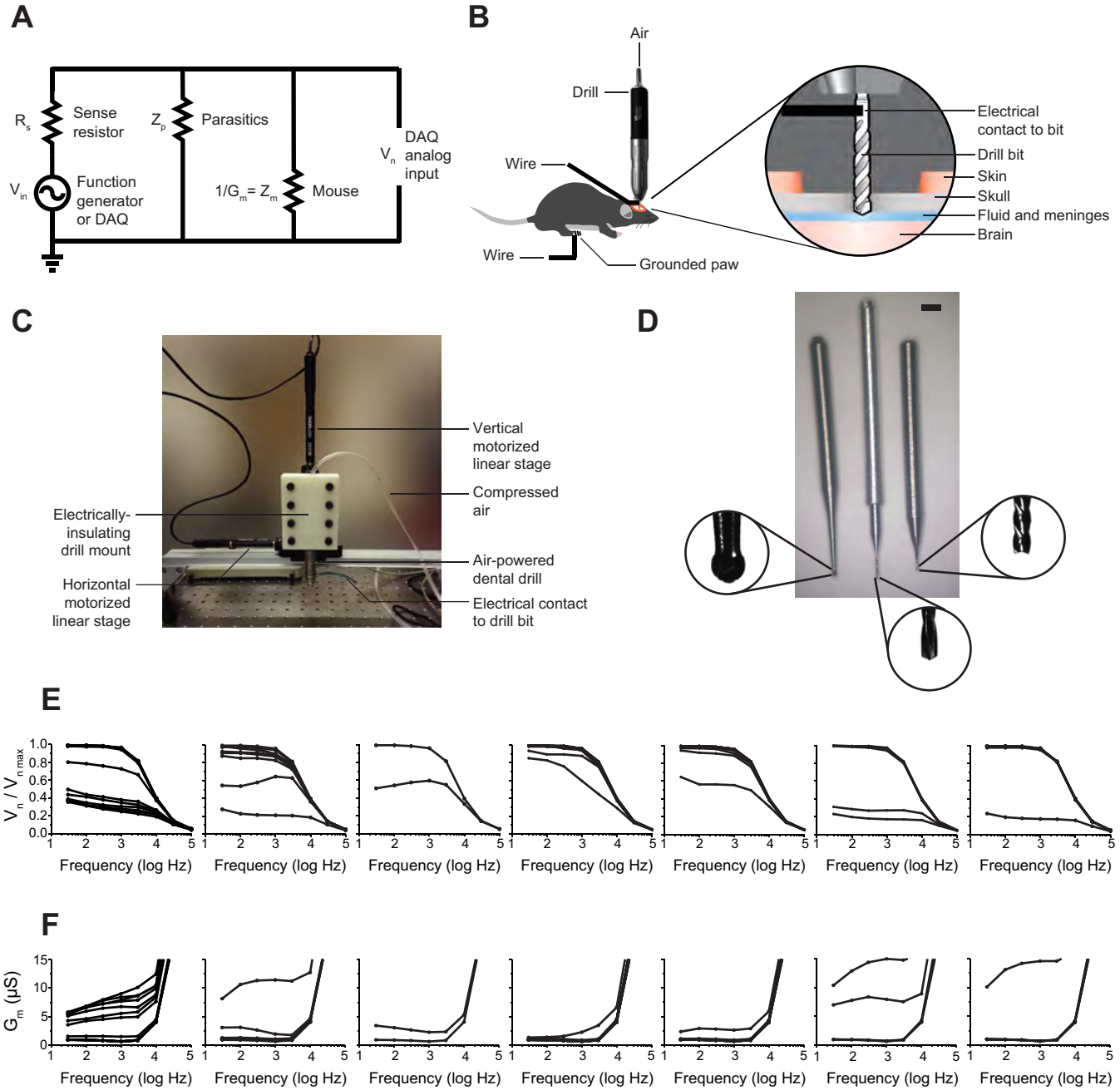

Fig. 1. Automated craniotomy robot design and implementation. *A*: diagram of electrical impedance measurement circuit. *B*: illustration of the experimental setup. *C*: photograph of the homebuilt automated craniotomy robot. *D*: drill bits used in this report, including a commercially available dental burr, 500 μm in diameter (*left*), a custom drill bit fusing a 200-μm tip with a custom aluminum dental drill adapter (*center*), and a custom 200-μm end mill created by using a lathe to turn down a commercially available bit (*right*). Scale bar, 1/16 in. *E*: normalized electric potential across the drill (acquired as schematized in *B* but with the electrical contact on the drill itself rather than the bit) and mouse, as a function of frequency, as a 500-μm dental burr is lowered into the skull for 7 different mice (step size: 10 μm for 6 mice, 50 μm for the 7th). Lower lines indicate lower drilling depth. *F*: electrical conductance vs. frequency (as in *E*) for all 7 mice. Higher lines indicate lower drilling depth.

The electric potential detection circuit relies on the ability to detect the change in the impedance across the mouse, Z_m. Figure 1*A* illustrates how this circuit works. The voltage drop across the sense resistor is $V_s = V_{in} - V_n$, and the current flow through the sense resistor is $i_s = V_s/R_s$. If parasitic currents, defined as $i_p = V_n/Z_p$, are present, e.g., via capacitive coupling of signal wires with grounded shielding in a cable, then some of the sense current flows through a parasitic impedance Z_p, calculated as the ratio V_n/i_s (measured when the mouse is not there). The current flow through the mouse, when present, is $i_m = i_s - i_p$. From these equations, the ratio of the voltage drop across the mouse to that of the input voltage, V_n/V_{in}, is calculated as $V_n/V_{in} = 1 - R_s(Z_p + Z_m)/[R_s(Z_p + Z_m) + Z_pZ_m]$. When the drill tip makes a hole in the skull, we found that Z_m decreases by five orders of magnitude, and this ratio decreases by about two orders of magnitude given a sense resistance of 10 MΩ.

To facilitate comparison across the multiple experimental setups explored here, e.g., different cables and different input voltages, we normalized the voltage across the mouse, V_n, by the maximum recorded voltage, $V_{n\,max}$, recorded in the open-loop configuration with no mouse in the circuit, before drilling began. The maximum recorded

Table 1. *Drilling parameters for homebuilt and modified commercial robots*

Figure	Electrical Contact	Sense Resistance	Driving Voltage	Driving Frequency	Cables	AC Signal Source	Measurement Device	$V_n/V_{n\ max}$ Threshold
1, *E* and *F*	Drill body	681 kΩ	20 V	30 Hz–100 kHz	Coaxial cable	Function generator	Oscilloscope	N/A
2	Drill body	681 kΩ	20 V	100 Hz	Twisted wire pair	Function generator	DAQ	N/A
3	Drill bit or end mill	10 MΩ	1 mV	100 Hz	Shielded USB	DAQ	DAQ	0.65 for drill bit (Fig. 3, *B*, *D*, and *E*), 0.45 for end mill (Fig. 3, *C*, *F*, and *G*)
4 and 5	Ball bearing	10 MΩ	1 mV	100 Hz	Individual wires	DAQ	DAQ	0.45 (only end mills used)

$V_n/V_{n\ max}$, voltage across mouse normalized by maximum recorded voltage; N/A, not applicable.

voltage is equal to the input voltage, when twisted pairs are used, or less for the case of parasitic currents, which occur with the coaxial and USB cables (see Table 1 to see which experiments used the coaxial vs. USB cables).

We always turned off the drill and waited for the drill to stop spinning before taking a measurement of the potential between the animal and the drill body (for Figs. 1 and 2) or drill bit (for Fig. 3). In the first iteration of the homebuilt system (Fig. 1, *E* and *F*, and Fig. 2), the impedance of the drill was included in the circuit because the simplest method for sending a signal through the drill initially appeared to be to connect a wire to the body of the drill, which is conductive to the drill bit. The impedance of the drill would show up as a resistor in series with the mouse in Fig. 1*A*. However, in later experiments (Fig. 3), the impedance of the drill was removed from the circuit by having a wire touch the shank of the drill bit directly (taking care not to apply excessive radial forces to the bit). This was done for two reasons: so that the largest potential drop across the mouse could be detected and because it was observed that the drill body impedance changed over time. We measured the impedance of the drill as ~50 KΩ new and 0.6–1.7 MΩ after some wear. We believe this is due to wear of the bearings that leads to an increase in contact resistance to the housing (i.e., race) of the bearings.

For Fig. 1, *E* and *F*, the drill was turned on manually, a step of 10 μm or 50 μm was taken (as explained in Fig. 1 legend), the drill was turned off, and a measurement was made after the drill came to a complete stop. For Figs. 2 and 3, a solenoid valve was used to activate the air supply to the drill for 300 μs, a step of 5 μm was taken, a pause of 3.5 s allowed the drill to come to a complete stop, and then a measurement was taken for 0.6 s.

As described in Table 1, different instruments were used to measure the electrical potential across the animal. For Fig. 2, some more detail may be helpful: the LabVIEW program extracted the maximum and minimum values of 10 sinusoids, each consisting of 1,500 samples at 25 kHz, and then subtracted the minimum value from the maximum for each sinusoid and averaged these 10 differences to estimate the peak-to-peak amplitude of the voltage drop across the mouse. For Fig. 3, the DAQ measured V_n in a different manner because we were using very low currents (as explained below), which would be within the noise. The LabVIEW program performed a partial discrete Fourier transform on V_n, calculating the amplitude of V_n as $\mathrm{sqrt}[\mathrm{Re}(X)^2 + \mathrm{Im}(X)^2]/N$, where $N = 15{,}000$ was the number of samples read and X was the coefficient of the sinusoidal component of the measured samples at the test frequency (100 Hz). X is defined as $X = \sum_{n=0}^{N-1} x_n e^{-i2\pi kn/N}$, where x_n is the nth measurement and k is calculated as N/[sampling rate (25 kHz) divided by the input frequency], which equates to the number of cycles that are recorded (in this case 60). $\mathrm{Re}(X)$ is calculated as $\sum_{n=0}^{N-1} x_n \cos(-2\pi kn/N)$, and $\mathrm{Im}(X)$ is calculated as $\sum_{n=0}^{N-1} x_n \sin(-2\pi kn/N)$.

We explored whether making a local measurement of impedance change was better than making a measurement across the body, as far as skull drilling detection was concerned. Measurements of the voltage with a ground electrode consisting of a skull screw (self-tapping

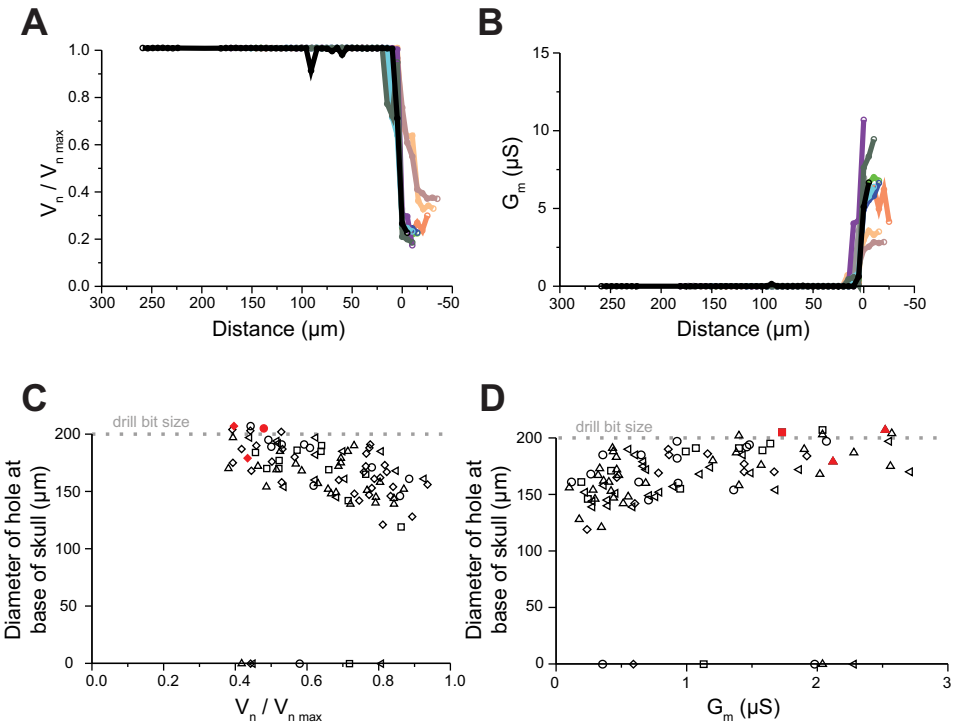

Fig. 2. The automated craniotomy threshold. *A*: normalized electric potential vs. distance traveled for 10 holes in 1 mouse skull, each represented by a different color (step size 5 μm, frequency 100 Hz). Traces were aligned (at x-axis = 0) at the point in the curve of maximum slope. *B*: electrical conductance vs. distance traveled (as in *A*) for all 10 craniotomies. *C*: hole size, measured at the base of the skull, measured with X-ray micro-computed tomography (CT), as a function of final normalized electric potential, with the drill stopping when various normalized electrical potentials were reached. $n = 98$ craniotomies in 5 mice; 200-μm drill bit (width indicated by dotted line). Each mouse is represented by a different shape, with red fill indicating visible blood related to the use of the standard pointed drill bit. For 6 of the 98 craniotomies the drill bit did not pass the bottom of the skull, and thus they are on the $y = 0$ line. *D*: hole size vs. electrical conductance for the data in *C*.

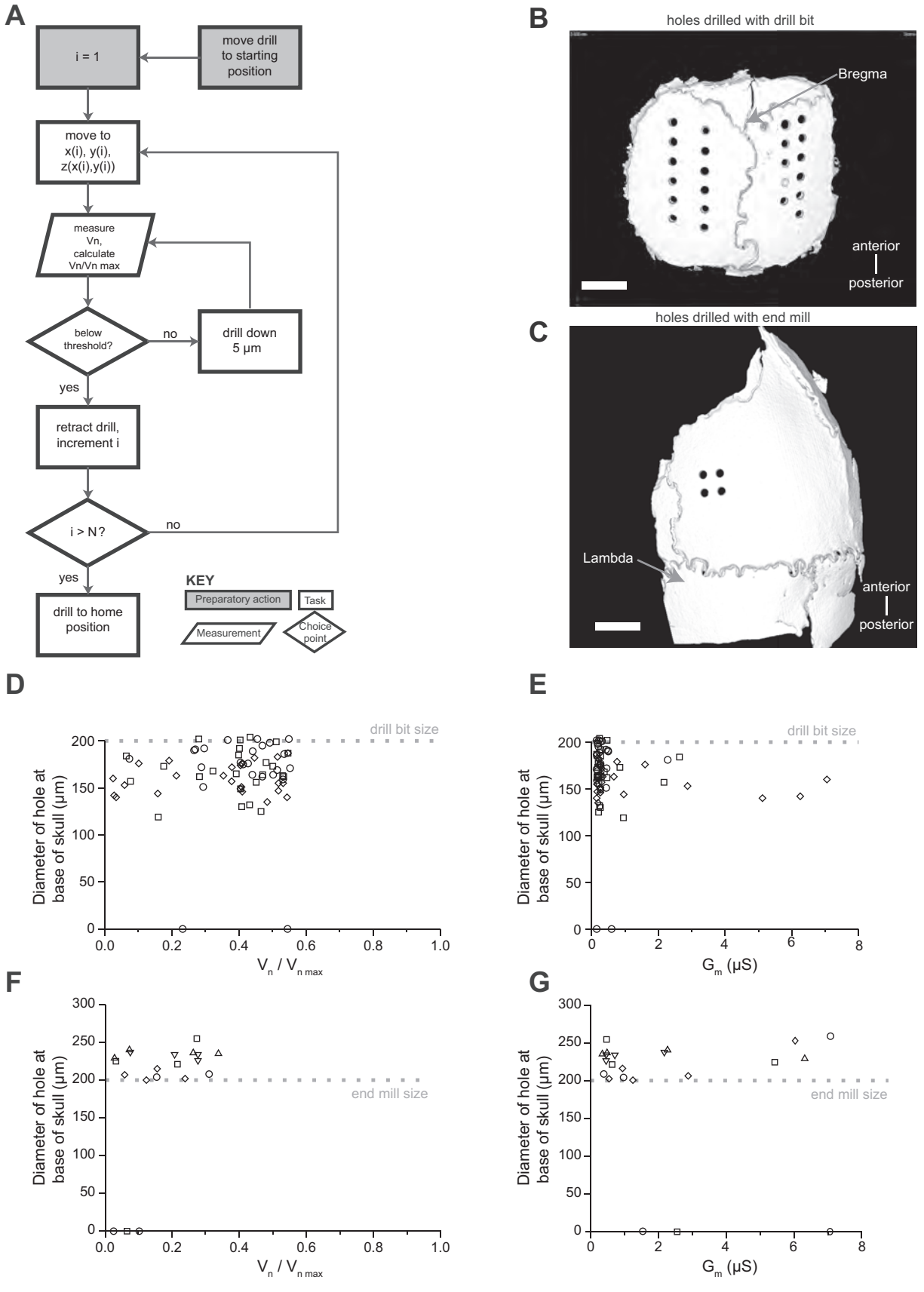

screw, size 000 thread, no. 303 stainless steel, 3/32-in. length; JI Morris, Southbridge, MA) inserted into a manually drilled craniotomy showed no improvement in the ability to detect a craniotomy opening by the robot drilling at a second site, presumably because the conductance through the body and through the brain are both high compared with the conductance of the skull.

Homebuilt system: mechanical design. The homebuilt system had a servo motor mounted on a three-axis translation stage that we assembled from three linear stages (Fig. 1*C*). These motors have a repeatable step size of 200 nm and a travel distance of 25 mm and are driven with LabVIEW commands. We usually used step sizes of 5 μm in the z direction, so the motor precision available was more than needed (and thus implementations severalfold cheaper than presented here might well be assembled; we used the motors thus chosen to allow exploration of the parameters of automated craniotomies). A common lab air supply was used to power the dental drill, and a solenoid valve (EV-2-6; Clippard, Cincinnati, OH) was connected between the air supply and the dental drill so that the dental drill could be turned on and off through a digital signal from the same LabVIEW program.

Dental drills are inexpensive and capable of extremely high rotary rates with minimal vibration, which is why they are popular in neuroscience for making small craniotomies. Most dental drills have a standard opening of 1/16 in. that fits commercially available dental burrs. These burrs range in size and shape but are only available down to 500 μm in diameter (Fig. 1*D*, *left*). Commercially available drill bits come in sizes of 200-μm diameter and less (McMaster-Carr) but have a 1-mm-diameter shank that is too small to fit into the dental drill. We wanted to create very small craniotomies, so we built an adapter that bridged this 1-mm to 1/16-in. gap in order to use these drill bits. To produce these adapters, a lathe was used to first drill a 1-mm hole in a 1/4-in.-diameter aluminum rod. Next, this rod was turned down with the lathe to an outer diameter of 1/16 in. and cut to 25 mm in length. The drill bits were then cut down to ~10 mm in length with a grinding tool, and the drill bit was then press fit into the adapter. One idea we explored was a custom-made chuck that would allow various diameter drill bits to be used with the dental drill. We abandoned this idea because we found that the high speed of the dental drill (up to a nominal 320,000 rpm) requires a precisely balanced chuck to eliminate vibrations; the adapters we produced are, in contrast, quite inexpensive (a few cents of material cost per adapter) and quick to produce (~15 min each).

The drill bits used here have a diameter of 200 μm and a point angle of 118°. This angled cutting edge means that for a fully bored hole in the skull the drill bit must penetrate 60 μm beyond the inner surface of the skull, increasing the risk of damage. This is an issue with all pointed drill bits used in neuroscience, not just those being used with dental drills. Similarly, the round burrs must protrude >100 μm beyond the inner surface of the skull for a fully bored-out 500-μm craniotomy. The round profile also results in inconsistent craniotomy size. Miniature square end mills (Harvey Tool, Rowley, MA) could in theory result in more consistent craniotomy openings but are not typically used in neuroscience applications. End mills with a 200-μm diameter and a 1/8-in. shank diameter were turned down by a machine shop (Contour360, Cornish, ME) to be able to fit into the 1/16-in. dental drill opening. Since these have a flat end, a fully bored-out craniotomy is created when the circuit detects breakthrough of the skull. For the same reason, these are potentially less damaging to the brain as well: since they are not pointed, they do not need to extend beyond the base of the skull to complete a full craniotomy. End mills also allow for cutting in all three directions, so more elaborate craniotomies can be created.

Modified commercial system: overview. To maximize community utilization of automatic craniotomy robots, we explored whether a commercially available craniotomy robot could be modified to utilize this closed-loop algorithm. We implemented the algorithm on a motorized stereotaxic robot (Neurostar, Tübingen, Germany). As purchased, the Neurostar was only capable of operating in "open-loop" mode, so we modified it to respond to changes in conductance at the drill tip (Fig. 4). We replaced the original drill with a micromotor carving drill (Ram Products, East Brunswick, NJ) to achieve faster rotation speeds (up to 45,000 rpm).

Modified commercial system: electrical circuit. The electric circuit for mouse voltage measurement of the modified commercial system was very similar to that of the homebuilt system. As seen in Fig. 4, the drill bit (a 200-μm end mill, Harvey Tool) was connected to a measurement circuit via a ball bearing (McMaster Carr part no. 60355K501) attached with conductive epoxy (MG Chemicals 8331) and filled with conductive carbon grease (MG Chemicals 846). This was done to eliminate the drill impedance from the circuit (analogous to the use of a wire to touch the drill bit for the homebuilt system; one method is not necessarily better than the other, but the ball bearing may be more robust over time because the wire can move). A second lead was connected to the animal by placing a wire beneath the scalp, or clipping it to a steel head plate if this was already in place for a previous experiment. The placement of the wire was based on convenience; we also tested this setup with a lead applied to the animal's paw, as in the homebuilt setup, which worked just as reliably. A data acquisition board (National Instruments USB-6001) sent a 1-mV, 100-Hz test signal through a 10-MΩ sense resistor while simultaneously measuring the voltage drop across the mouse with a 10-kHz sampling rate. Measurements were taken with a National Instruments data acquisition board (Fig. 4*B*) at a rate of 2 Hz, with each measurement lasting 100 ms. The drill was moved down in 5-μm increments after every other measurement. As in the measurement circuit from the homebuilt system, if V_n dropped below a threshold of $0.45 \times V_{n\ max}$ (computed via the fast Fourier transform of the incoming signal), the drill was retracted to its starting position. Sending the test signal through a ball bearing (Fig. 4*D*) made it possible to take measurements without stopping the drill, speeding up the drilling process by an order of magnitude.

The Neurostar and the data acquisition board were both controlled by a custom Python graphical user interface (GUI), written with the PyQt4, PyDAQmx, and PyUSB libraries. Schematics, parts lists, and software for this setup can also be found at **http://autosurgery.org**.

Modified commercial system: mechanical design. The Neurostar contains three separate stepper motors, one for each axis of movement in a standard sterotaxic frame (Fig. 4*A*). These motors are attached to a Kopf model 900 Small Animal Stereotaxic Instrument (David Kopf Instruments, Tujunga, CA). Each motor is connected to a control unit, which is in turn connected via a USB interface to a computer. We replaced the Neurostar software with a custom GUI written in Python. This software can be used to control the drill manually, as in the Neurostar software, or to set it into "closed-loop" mode, which can stop the drill when conductance measurements indicate that the drill tip has broken through the skull. In addition, we have created an interface for drilling more complex patterns, such as cranial windows

Fig. 3. Implementation and validation of automated craniotomy algorithm. *A*: automated craniotomy algorithm flowchart. *B*: representative CT scan of a skull from *D*. Scale bar, 1 mm. *C*: representative CT scan of a skull from *F*. Scale bar, 1 mm. *D*: hole size as a function of final stopping normalized electric potential for 72 craniotomies in 3 mice with a 200-μm drill bit, step size of 5 μm, and normalized electrical potential threshold of 0.65. Each mouse is represented by a different shape. For 2 of the 72 craniotomies the drill bit did not pass the bottom of the skull, and thus they are at the $y = 0$ line. *E*: hole size vs. electrical conductance for the data in *D*. *F*: hole size as a function of final stopping normalized electric potential for 20 craniotomies in 5 mice with a 200-μm flat-end end mill, step size of 5 μm, and normalized electrical potential threshold of 0.45. Each mouse is represented by a different shape. For 3 of the 20 craniotomies the drill bit did not pass the bottom of the skull, and thus they are at the $y = 0$ line. *G*: electrical conductance vs. hole size for the data in *F*.

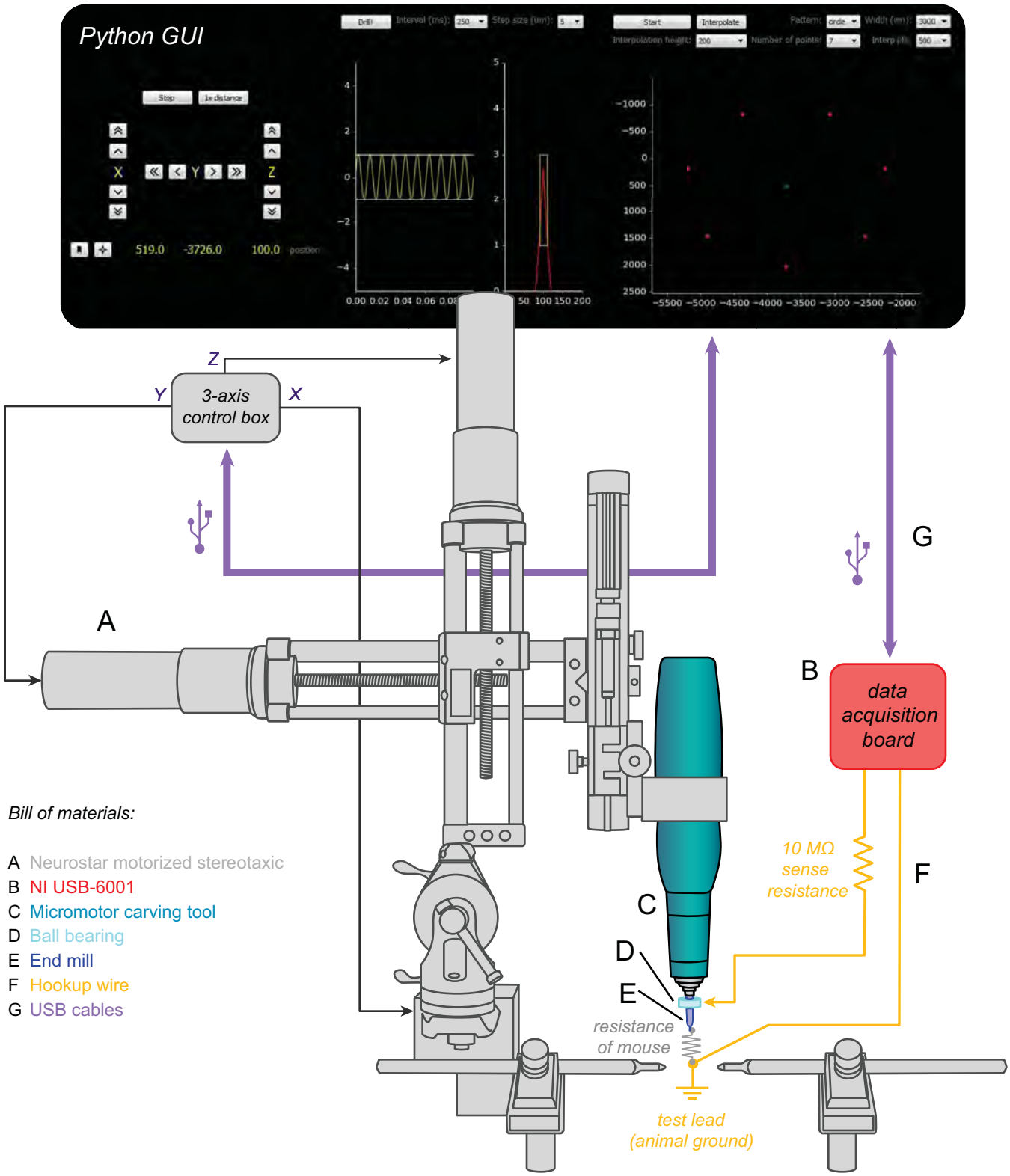

Fig. 4. Implementation of automated craniotomy algorithm on a commercial motorized stereotaxic. A graphical user interface (GUI, *top*) controls the movement of the stereotaxic frame (*A*) via a 3-axis control box. A micromotor carving drill (*C*) with adjustable rotation speeds up to 45,000 rpm is attached to the stereotaxic via a custom adapter. The drill turns an end mill (*E*) with a tip diameter of 200 μm. When the end mill breaks through the skull, it completes the circuit formed between a wire carrying the 100-Hz test signal from a data acquisition board (*B*) and a test lead connected to the animal (*F*). The signal wire is attached to the drill bit via a ball bearing (*D*), allowing continuous impedance testing without the need to stop the drill.

of varying diameters. The robotic drill remains compatible with the Neurostar software, for example, if users wish to take advantage of its integrated 3D atlas. However, the Neurostar software, which can only control the robot in "open-loop" mode, cannot be used simultaneously with our "closed-loop" Python GUI software, as each program needs full control of the USB communication channel in order to operate. One can, if desired, first use the Neurostar software to localize craniotomies with its 3D atlas and then switch over to our Python GUI to run the drill in closed-loop mode for precision craniotomy creation.

The stepper motors operate by rotating the shaft of the Kopf stereotaxic positioner to drive movement along that axis, much in the same way an operator would use the same manual stereotaxic frame. We measured the standard deviation of the specified steps to be 1.8 μm for the rostral-caudal (x) axis, 2.0 μm for the medial-lateral (y) axis, and 1.2 μm for the dorsal-ventral (z) axis. The range of travel along each axis is 70 mm, which is slightly more limited than that of the Kopf frame, to protect the motors from damage.

We replaced the Neurostar drill with an electrical micromotor carving tool (Ram Products) (Fig. 4*C*) capable of achieving higher rotation speeds (up to 45,000 rpm) and accommodating square end mills with shank diameters of 1/8 in. (Fig. 4*E*). This alleviated the need to modify the end mills but did require a custom adapter for attaching the drill to the stereotaxic frame.

Large cranial windows were created by drilling a series of test holes around the edge of the desired window (Fig. 5*A*). Unlike manually created cranial windows that rely on operator feel to determine when enough skull has been removed (Holtmaat et al. 2009; Mostany and Portera-Cailliau 2008), each hole was used to determine the location of the inner surface of the skull at each point, in order to obtain a 3D representation of skull curvature. When the drill broke through the skull (as indicated by a change in conductance), the depth of the drill tip was recorded to obtain a z position for each x-y hole location. For 3-mm-diameter windows, we used a total of seven evenly spaced test holes. The number of holes can be adjusted as needed for larger or smaller windows. Once all of the test holes were drilled, the custom Python GUI computed a skull surface profile based on cubic spline interpolation of the x, y, and z coordinates of each hole (500 points per axis). At this point, the software switched from "closed-loop" to "open-loop" mode: the drill traced a path of overlapping holes without measuring conductance. We avoided damage to the underlying tissue by stopping a distance of 20 μm above the measured z depths (Fig. 5*B*). If the drill does not go deep enough on the first pass, the user can manually select individual segments to be redrilled at a different depth. The two steps in this procedure that required manual intervention were the initial alignment of the drill bit with the center of the desired window and the removal of the circular bone fragment under saline. In between these steps, the robot operated independently.

In our experiments we created circular cranial windows for optical imaging, but a similar technique could be used to create windows of different shapes. For example, a rectangular window would require test holes to be drilled at several points along each edge; the exact number would depend on the overall size of the window. The software would need to be modified to enable spline interpolation along individual edges, rather than between all of the test holes, to keep the corners of the window square. As our software is open source, such changes are easy to implement.

Considerations on electrical current. We wanted to ensure that the maximum electrical current through the body (equal to the amplitude of the injected sine wave divided by the sense resistance) was small enough (~100 pA) to avoid brain stimulation. Therefore, a 1-mV amplitude of the sine wave and a 10-MΩ sense resistor were chosen for the final iteration of the homebuilt system (Fig. 3), as well as the modified commercial system (Fig. 4, Fig. 5). With the cross-sectional area of a 200-μm-diameter cylinder as the electrode area of the drill bit, the current density was ~0.0032 A/m^2, nearly two orders of magnitude less than the lowest current densities (0.28 A/m^2) capable of stimulating brain tissue (Brunoni et al. 2012; Chaieb et al. 2011; Nitsche et al. 2003). Furthermore, this current was only applied across the brain for a few seconds during the drilling operation. Finally, the signal processing methods used above could in principle be used to lower the current further, if desired.

Animal surgeries. All procedures were in accordance with the National Institutes of Health *Guide for the Care and Use of Laboratory Animals* and were approved by the Massachusetts Institute of Technology (MIT) and Allen Institute for Brain Science animal care and use committees. For experiments performed at MIT, 2- to 5-mo-old C57BL/6 wild-type mice (male) were given general anesthesia with a rodent anesthesia machine and 2% isoflurane in pure oxygen. Animals were placed on a heating pad with a temperature probe to maintain body temperature. After fully nonresponsive to foot withdrawal reflex test, mice were administered the analgesics buprenorphine (0.1 mg/kg) and meloxicam (1–2 mg/kg) subcutaneously. Mice were immobilized in a stereotaxic apparatus (Kopf model 900) with ear bars and a nose holder and bite bar. With a scalpel an incision was made on the scalp to expose the skull, and then the skin was retracted with clips. We used a small curette to retract or remove residual fascia or connective tissue over the area of interest of the skull. Calibrating the stereotaxic coordinates can be performed by moving the drill tip to bregma or lambda for a well-aligned mouse in a stereotaxic frame and then zeroing the coordinates in our custom software (either LabVIEW or Python). Experiments lasted up to 2 h, with saline added to soft tissues (with the skull dry so as to present a constant impedance). Experiments were terminal. For experiments performed at the Allen Institute, all procedures were identical except that subcutaneous analgesics were not administered.

Thermocouple evaluation. We automatically drilled a 3-mm cranial window using the technique described above in order to place a thermocouple probe beneath the skull. We used the modified commercial robot to drill four holes in closed-loop mode, moving the tip of the probe each time to ensure that it was directly below each hole. Baseline and maximum temperature measurements (in °C) were read from a multimeter (Fluke, Everett, WA) and recorded manually.

CT evaluation. After the end of each experiment performed with the homebuilt system, skulls were removed and craniotomy diameters were measured with an X-ray micro-computed tomography (CT) system (XT H 160, Nikon, Tokyo, Japan). Additionally, the CT scanner was used to get a measurement for the distance between the inner surface of the skull and the brain. With CT reconstructions from an unrelated experiment in which the entire head of a mouse was scanned, this distance was measured to be on the order of 40–60 μm.

RESULTS

Derivation of automated craniotomy algorithm. We first derived the automated craniotomy algorithm. Impedance measurements showed that when the drill tip came in contact with the skull surface the observed electrical current across the body was negligible, because of the small conductance of the skull (<0.10 nS; measured with an LCR meter, 4263B, Agilent, Santa Clara, CA). However, when the drill tip penetrated the skull the conductance between the drill bit and the body dramatically increased because of the high conductivity of cerebrospinal fluid. To find the frequency of voltage applied that resulted in the largest electric potential drop, we delivered various sinusoidal test signals to the drill and measured the voltage amplitude and phase angle across the mouse as a 500-μm-diameter dental burr was passed through the skull. We found that the voltage was sensitive to drill depth through the skull over a range of frequencies from 30 Hz to 1 kHz ($n = 7$ mice; Fig. 1*E*, voltage data; Fig. 1*F*, calculated conductance data). On the basis of these data, we chose a frequency of 100

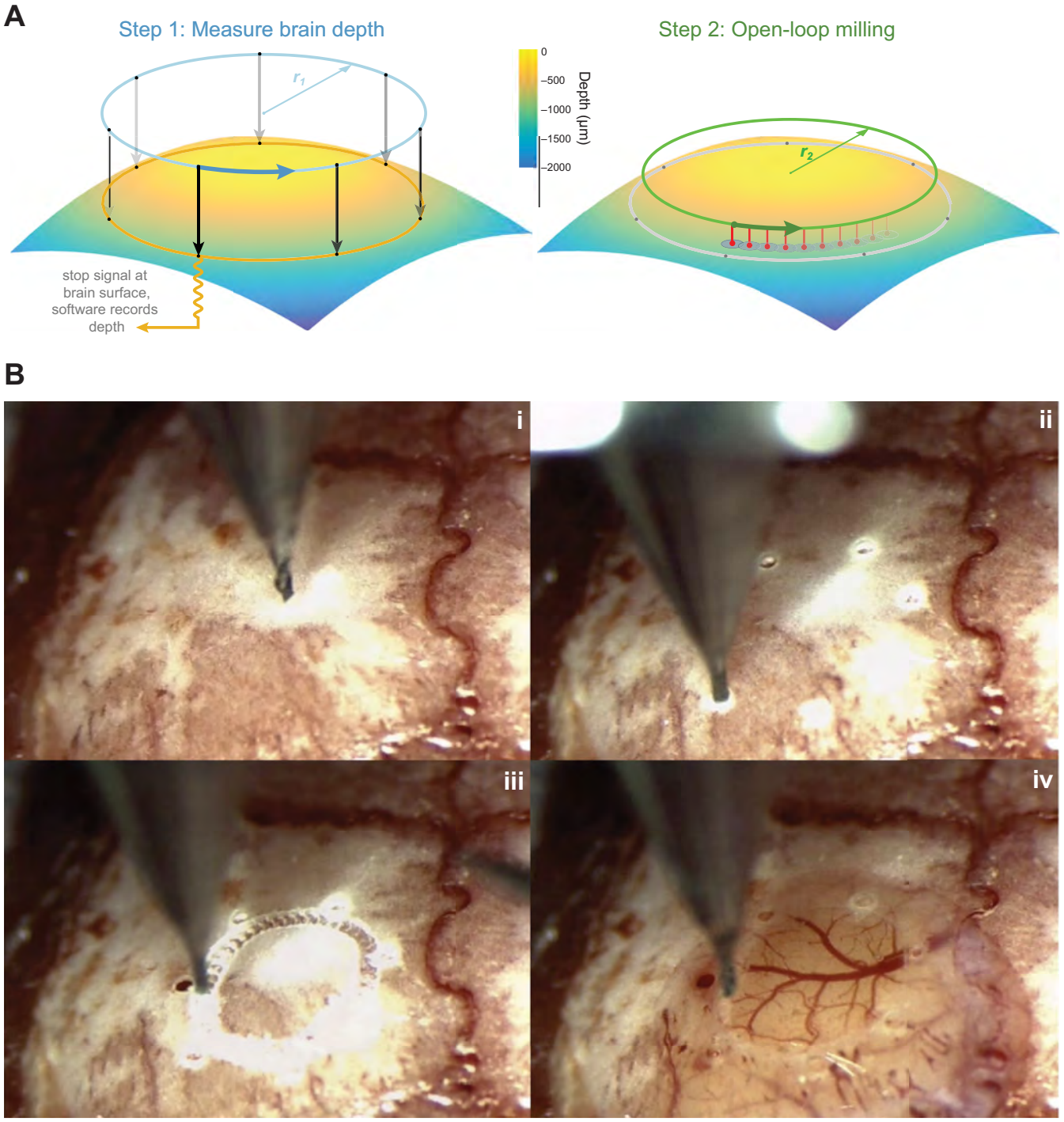

Fig. 5. Automated formation of large cranial windows. *A*: windows are created after drilling a series of test holes to account for the curvature of the skull (*left*). In this example, holes are drilled at 7 points along the circumference of a 3-mm circle (dots). Impedance-based feedback is used to measure the location of the brain along the *z*-axis at each point. Then, cubic spline-based interpolation is used to compute the optimal path for the drill to create a circular pattern in the bone without contacting the underlying tissue (*right*). The best results were achieved when the drill made a series of shallow, overlapping holes (red) rather than milling horizontally through the bone. *B*: the steps involved in creating a cranial window in an actual mouse skull (see Supplemental Movie S1 for a video of the windowing process). *i*: The skull is exposed and cleaned. *ii*: The center point and diameter of the desired cranial window are manually chosen by the surgeon, and several holes are automatically drilled along its circumference. *iii*: The drill automatically interpolates between the hole locations at the appropriate depth. *iv*: The skull is manually removed under saline.

Hz because it showed a large electric potential drop as the drill bit passed through the skull.

Having determined that 100-Hz sinusoidal voltage was sufficient to detect skull penetration, we next sought to determine whether we could characterize the conductance as a function of drill depth in order to find a clear threshold that indicated when to stop drilling. To do that, we examined the time course of the conductance changes as the drill advanced through the skull (Fig. 2, *A* and *B*; $n = 10$ holes in 1 mouse skull). We observed that (for each craniotomy) conductance is near zero for most of

the drilling process, then jumps significantly to a higher value over a small number of steps, and then remains high for subsequent steps of the drill. This indicated that conductance does not vary appreciably as the skull is thinned but instead rises suddenly when the drill passes slightly through the inner surface of the skull. We sought to determine whether a precise threshold for the conductance could be derived, so that the robot would stop when it completed the craniotomy without damaging the brain. We ran the robot with a 200-μm drill bit, stopping the drilling when various electrical potentials (Fig. 2*C*, normalized as described in METHODS; Fig. 2*D*, calculated conductances) were achieved. For each trial, we measured the craniotomy diameter at the base of the skull with the CT scanner. As the normalized electrical potential threshold was lowered systematically (from ~0.95 to ~0.3), the hole diameters increased, from under 150 μm to around 200 μm ($n = 98$ craniotomies in 5 mice). The electric potential and hole diameter were inversely correlated (Fig. 2*C*, correlation coefficient $r = -0.61$, $P = 1.26 \times 10^{-7}$), with lower potential being associated with larger hole diameters. In 6 of the 98 cases, the experiment was stopped because of hitting a blood vessel in the skull—a benign, occasional event that yielded zero-diameter holes. In a small minority of cases, the drill successfully created a craniotomy but produced bleeding, suggesting that the standard use of a pointed drill bit yields a suboptimal craniotomy (red symbols, Fig. 2, *C* and *D*). We chose a threshold for our drill high enough so that bleeding could be avoided but small enough to maximize hole size. For the particular 200-μm-diameter drill bits that were used in these experiments, we found that a normalized electric potential threshold value of 0.65 yielded a good balance.

Once we had discovered that a threshold could be defined that balanced craniotomy success and safety, we implemented an algorithm to perform electric potential measurements over time while a drill was lowered through the skull in 5-μm steps, halting motion when the drill-to-body potential dropped below the threshold (Fig. 3*A*). Across multiple trials of our homebuilt craniotomy robot and algorithm, we found that craniotomies could be reliably drilled (Fig. 3*B*) with the normalized electric potential threshold of 0.65 derived above (Fig. 3, *D* and *E*; $n = 72$ craniotomies in 3 mice). For six of the craniotomies, minor bleeding was observed from the skull after drilling to only a shallow depth (implying again that a blood vessel in the skull had been hit). For four of these cases, waiting a minute or so for the blood to clot was sufficient to allow the procedure to continue to the point of a complete craniotomy at a later time. Waiting and redrilling the remaining two craniotomies was not attempted and might have allowed the successful creation of craniotomies in those locations as well.

Implementation of automated craniotomy formation with a simple homebuilt robot. Having derived and validated the automated craniotomy algorithm, we now set out to see whether it were possible to develop a practical robot that could drill essentially perfect craniotomies. In addition, the holes drilled in Fig. 3, *D* and *E*, were typically less than the width of the drill bit, because the pointed tip would break through before the wider shaft, resulting in a not completely bored-out hole. As noted above, the use of a pointed or rounded drill bit, although popular in neuroscience, may also result in part of the drill projecting significantly below the skull base, potentially injuring the brain. We created (see METHODS) blunt-tipped end mills of 200-μm diameter that could be used in a dental drill (Fig. 1*D*, *right*) and changed the threshold used (Fig. 3*A*) to a lower value, 0.45, derived from the threshold evaluation plots (Fig. 2, *C* and *D*). We found that truly cylindrical holes (Fig. 3*C*) could now be made, with diameters equal to or larger than the end mill diameter ($n = 20$ craniotomies in 5 mice; Fig. 3, *F* and *G*). For 3 of the 20 craniotomies, skull bleeding was observed; in principle these could have been allowed to continue as in Fig. 3, *D* and *E*, after a brief waiting period to allow clotting. Craniotomy sizes of >200 μm were due to some end mills not being perfectly concentrically machined down in the manufacturing process used to modify the end mills (see METHODS).

The normalized electric potential thresholds used here are the best values we found for the bits used in our experiments. Having tried other sized bits (300-μm pointed tip drill bits and 300-μm flat end mills), we believe that these threshold values should work in general but may require slight adjustments. The cause of such adjustments in threshold value is due to the curvature of the skull and the geometry of the bit, which both affect how much of the bit breaks through the skull before an impedance measurement can be made.

For the end mill experiments, we characterized the precision of the craniotomy robot. We created four craniotomies in an array, with 500-μm spacing (center to center) in both the anteroposterior and mediolateral directions. The measured center-to-center distance was 496 ± 6 μm (mean ± SD, $n = 10$ pairs of craniotomies, including the partial craniotomies) in the mediolateral direction and 492 ± 10 μm in the anteroposterior direction. These errors approach the resolution of the CT scanner used to image the skulls (~5 μm).

Modifying a commercial robot to do automated craniotomies. To maximize the accessibility of automated craniotomies, we explored whether a commercially available craniotomy robot, which normally operates in open-loop mode, could also be modified to utilize this closed-loop algorithm. We modified a Neurostar stereotaxic robot (Fig. 4) and found it was capable of creating reliable, clean craniotomies with the same conductance-based feedback algorithm. In addition, we used this system to create larger cranial windows up to 5 mm in diameter ($n = 12$, 3-mm windows in 10 mice; $n = 3$, 5-mm windows in 3 mice). An example is shown in Fig. 5*B* and Supplemental Movie S1.[1] Using a 200-μm square end mill, we drilled a series of test holes around the circumference of the desired window (Fig. 5*Bii*). Based on the measured *x*, *y*, and *z* coordinates of each hole, we drilled a series of shallow, overlapping holes along a path that accounted for the curvature of the skull (Fig. 5*Biii*). The bone fragment was then removed under saline, exposing the brain underneath (Fig. 5*Biv*). The entire process took ~15 min for each window (10 min to drill the test holes at 1 min and 20 s per hole and 5 min to open the window). In some instances, the drill passed through a skull vessel, causing bleeding that quickly subsided.

We placed a thermocouple directly beneath the skull to measure potential heating effects of drilling, using the modified commercial robot in closed-loop mode. Using a 5-μm step size and a 500-ms pause between steps, we measured a maximum temperature increase of 2.5°C under the drill bit. Since the

[1] Supplemental Material for this article is available online at the Journal website.

brain below the exposed skull started out cooler than the mouse's average body temperature (Kalmbach and Waters 2012), with a temperature of 25.6 ± 0.27°C ($n = 4$ baseline readings), we never observed heating above core body temperature (37°C). If desired, such temperature could be mitigated by blowing appropriate-temperature air over the skull surface during the drilling process (taking care to avoid soft tissue desiccation). When the drill is running in open-loop mode (as during the second step of the windowing process; Fig. 5*A*), saline could be placed on the skull surface to regulate temperature and prevent tissue dehydration.

DISCUSSION

Here we report that a drill bit passing through the mouse skull encounters a stereotyped increase in conductance with respect to the mouse body. We developed an algorithm based on this information to detect skull breakthrough and constructed both homebuilt as well as modified commercially available robotic devices that utilize this algorithm to perform automated craniotomies with high precision, high yield, and good safety, with the ability to stop with ~5-μm resolution. We did not observe brain bleeding in any of the trials performed by our robot with the conductance thresholds determined. Bleeding can alter cortical physiology (Shih et al. 2013), and release of blood can affect neural signaling (Regan and Guo 1998; Yip et al. 1996). Our precise control of drill depth obviates such concerns.

The use of craniotomy robots with this skull breakthrough detection algorithm allows many small precisely spaced craniotomies to be drilled, which may be useful for deploying multi-injector (Chan et al. 2010), multi-electrode (Maynard et al. 1997; Recce and O'Keefe 1989; Scholvin et al. 2015), or multi-optical fiber (Zorzos et al. 2012) probes for interrogating distributed neural circuits. Although this is currently possible with robotic drills operated in manual mode (e.g., the Neurostar drill), adding conductance-based feedback speeds up the process by introducing closed-loop feedback of skull breakthrough detection. The smallest size of craniotomy possible with the technique presented here is limited by the size of available bits, which currently go down to 50 μm, but it may be possible to create custom tools that are even smaller. It is difficult for human surgeons to handle drill bits of this size, making a robotic device a practical solution when holes of this size are desired.

Automated craniotomies have been attempted before. Some methods used force feedback or related signals to halt drill motion (Loschak et al. 2012; Pohl et al. 2011), and others used an open-loop device without feedback (Cunha-Cruz et al. 2010). However, it is unclear whether these methods can achieve better than millimeter resolution. Open-loop systems require CT scanning of the skull to measure the skull thickness, which is both expensive and involves X-rays. Still others use femtosecond lasers to ablate the skull, again, an expensive proposition (Jeong et al. 2013). In contrast, our method achieves precision in the micrometer range, and without requiring elaborate X-ray or laser technology.

Our method for automated opening of craniotomies will be accessible to a wide range of neuroscientists. We have shown that the algorithm works equally well on homebuilt (Fig. 1) and modified commercial (Fig. 4) systems. While the performance of the homebuilt and modified commercial system was comparable, for most users the modified commercial system will be faster and easier to set up. The benefit of the homebuilt system is the ability to choose components to optimize the cost and performance. A basic automated craniotomy robot could be built for under $1,000, with the highest cost component being the drill. Both setups offer the ability to align the drill tip with specific stereotaxic coordinates, although the modified commercial system has the advantage of integrated 3D atlas visualization provided via the Neurostar software.

Because our technique is conceptually simple, it should be straightforward to adapt it to alternate setups. Although we have only drilled automated craniotomies in mice, our setup may also be of interest to scientists working with other mammals, such as rats and rhesus macaques. Our procedure could in principle allow experimenters to create more precise openings in thick skulls, with less chance of damaging underlying brain tissue, while reducing the time required to train surgeons to work with new species. Threshold values will of course likely vary for different species because the body conductance will vary; it may also make sense to use larger-diameter end mills for larger animals.

Automated craniotomies, of course, do not replace human surgeons: our method still requires a human to place the mouse in a stereotaxic device, expose the skull, and align the drill with appropriate structures. However, using our technique for automated craniotomies should result in more consistent holes with smaller diameters and tighter spacing than previously possible. Furthermore, the opening of large cranial windows—something that typically requires extensive training—can now be performed by novice surgeons. A single experimenter may be able to operate multiple surgical robots in parallel. As the tools for neural recording and stimulation become increasingly sophisticated, it is important to eliminate variability in craniotomy quality as a potential failure mode for these devices. The use of conductance-based feedback is an effective way to improve the reliability of the holes needed to expose the brain prior to inserting pipettes, electrodes, and fiber-optic cables, or for the purpose of imaging neural tissue.

ACKNOWLEDGMENTS

We thank members of the Allen Institute for Brain Science, the MIT Media Lab, and the MIT McGovern Institute. We acknowledge B. Allen for CT data used to measure the skull to brain distance.

GRANTS

This work was supported by a National Science Foundation (NSF) Graduate Fellowship (N. Pak). This work was funded in part by the Allen Institute for Brain Science. E. S. Boyden was funded by the National Institutes of Health (NIH) Director's Pioneer Award 1DP1 NS-087724 and Transformative Award 1DP1 NS-087724, NIH Single Cell Grant 1R01 EY-023173, the New York Stem Cell Foundation-Robertson Award, NSF CBET 1053233, the IET Harvey Prize, and NSF Cognitive Rhythms Collaborative DMS 1042134. The authors thank the Allen Institute founders, Paul G. Allen and Jody Allen, for their vision, encouragement, and support.

DISCLOSURES

No conflicts of interest, financial or otherwise, are declared by the author(s).

ENDNOTE

At the request of the authors, readers are herein alerted to the fact that additional materials related to this manuscript may be found at the institutional

website of one of the authors, which at the time of publication they indicate is: http://autosurgery.org. These materials are not a part of this manuscript, and have not undergone peer review by the American Physiological Society (APS). APS and the journal editors take no responsibility for these materials, for the website address, or for any links to or from it.

AUTHOR CONTRIBUTIONS

Author contributions: N.P., J.P.K., T.J.B., and E.S.B. conception and design of research; N.P., J.H.S., J.P.K., and D.J.D. performed experiments; N.P., J.H.S., J.P.K., D.J.D., T.J.B., and E.S.B. analyzed data; N.P., J.H.S., J.P.K., D.J.D., T.J.B., and E.S.B. interpreted results of experiments; N.P., J.H.S., J.P.K., and E.S.B. prepared figures; N.P. and J.P.K. drafted manuscript; N.P., J.H.S., J.P.K., T.J.B., and E.S.B. edited and revised manuscript; N.P., J.H.S., T.J.B., and E.S.B. approved final version of manuscript.

REFERENCES

Brunoni AR, Nitsche MA, Bolognini N, Bikson M, Wagner T, Merabet L, Edwards DJ, Valero-Cabre A, Rotenberg A, Pascual-Leone A, Ferrucci R, Priori A, Boggio PS, Fregni F. Clinical research with transcranial direct current stimulation (tDCS): challenges and future directions. *Brain Stimul* 5: 175–195, 2012.

Chaieb L, Antal A, Paulus W. Transcranial alternating current stimulation in the low kHz range increases motor cortex excitability. *Restor Neurol Neurosci* 29: 167–175, 2011.

Chan SY, Bernstein JG, Boyden ES. Scalable fluidic injector arrays for viral targeting of intact 3-D brain circuits. *J Vis Exp* 35: 1489, 2010.

Cunha-Cruz V, Follmann A, Popovic A, Bast P, Wu T, Heger S, Engelhardt M, Schmieder K, Radermacher K. Robot- and computer-assisted craniotomy (CRANIO): from active systems to synergistic man-machine interaction. *Proc Inst Mech Eng H* 224: 441–452, 2010.

Holtmaat A, Bonhoeffer T, Chow DK, Chuckowree J, De Paola V, Hofer SB, Hübener M, Keck T, Knott G, Lee WC, Mostany R, Mrsic-Flogel TD, Nedivi E, Portera-Cailliau C, Svoboda K, Trachtenberg JT, Wilbrecht L. Long-term, high-resolution imaging in the mouse neocortex through a chronic cranial window. *Nat Protoc* 4: 1128–1144, 2009.

Jeong DC, Tsai PS, Kleinfeld D. All-optical osteotomy to create windows for transcranial imaging in mice. *Opt Express* 21: 23160–23168, 2013.

Kalmbach AS, Waters J. Brain surface temperature under a craniotomy. *J Neurophysiol* 108: 3138–3146, 2012.

Kodandaramaiah SB, Franzesi GT, Chow BY, Boyden ES, Forest CR. Automated whole-cell patch-clamp electrophysiology of neurons in vivo. *Nat Methods* 9: 585–587, 2012.

Loschak P, Xiao K, Pei H, Kesner SB, Thomas AJ, Walsh C. Cranial drilling tool with retracting drill bit upon skull penetration. In: *Proceedings of the Design of Medical Devices Conference, April 10–12, 2012*, Minneapolis, MN: University of Minnesota Medical Devices Center, 2012.

Maynard EM, Nordhausen CT, Normann RA. The Utah intracortical electrode array: a recording structure for potential brain-computer interfaces. *Electroencephalogr Clin Neurophysiol* 102: 228–239, 1997.

Mostany R, Portera-Cailliau C. A craniotomy surgery procedure for chronic brain imaging. *J Vis Exp* 12: 18–19, 2008.

Nitsche MA, Liebetanz D, Lang N, Antal A, Tergau F, Paulus. Safety criteria for transcranial direct current stimulation (tDCS) in humans. *Clin Neurophysiol* 114: 2220–2222, 2003.

Pohl BM, Schumacher A, Hofmann UG. Towards an automated, minimal invasive, precision craniotomy on small animals. In: *Proceedings of the 5th International IEEE EMBS Conference on Neural Engineering, April 27-May 1, 2011*, Cancun, Mexico, 2011.

Recce M, O'Keefe J. The tetrode: a new technique for multi-unit extracellular recording (Abstract). *Soc Neurosci Abstr* 19: 1250, 1989.

Regan RF, Guo Y. Toxic effect of hemoglobin on spinal cord neurons in culture. *J Neurotrauma* 15: 645–653, 1998.

Scholvin J, Kinney JP, Bernstein JG, Moore-Kochlacs C, Kopell N, Fonstad CG, Boyden ES. Close-packed silicon microelectrodes for scalable spatially oversampled neural recording. *IEEE Trans Biomed Eng* 99: 1, 2015.

Shih AY, Blinder P, Tsai PS, Friedman B, Stanley G, Lyden PD, Kleinfeld D. The smallest stroke: occlusion of one penetrating vessel leads to infarction and a cognitive deficit. *Nat Neurosci* 16: 55–63, 2013.

Yip S, Ip JK, Sastry BR. Electrophysiological actions of hemoglobin on rat hippocampal CA1 pyramidal neurons. *Brain Res* 713: 134–142, 1996.

Zorzos AN, Scholvin J, Boyden ES, Fonstad CG. Three-dimensional multiwaveguide probe array for light delivery to distributed brain circuits. *Opt Lett* 37: 4841–4843, 2012.